C. R. Physique 14 (2013) 425–437

Contents lists available at SciVerse ScienceDirect

Comptes Rendus Physique

www.sciencedirect.com

Electromagnetic fields: from dosimetry to human health

Multi-sensors SAR system for real-time dosimetry assessment

Christian Person [a,*], Gaëtan Guevel [a], Joe Wiart [b], Yann Toutain [c], Romain Butet [c], Sylvie Le Dall [c]

[a] Whist-Lab/Lab-STICC, Telecom Bretagne, CS 83818, 29238 Brest, France
[b] Whist-Lab/Orange Labs, Orange Labs, 38-40, rue du Général-Leclerc, 92794 Issy-les-Moulineaux, France
[c] Satimo Bretagne, Microwave Vision, ZI du Vernis, 225, rue Pierre-Rivoalon, 29200 Brest, France

ARTICLE INFO

Article history:
Available online 29 March 2013

Keywords:
SAR measurement
E-field probes
Electromagnetic analysis
No-robot SAR test bench
Calibration
Real-time dosimetry

ABSTRACT

A multi-sensor test-bench for determining the SAR (specific absorption rate) due to wireless devices emitting in equivalent human tissues is presented. Real-time SAR assessment is proposed considering a spatially distributed multiprobe test-bench. In comparison with a multi-axial robot SAR system, the proposed one does not require any displacement, thus reducing drastically acquisition time, once parallel data acquisition and interpolation techniques are employed for accelerating measurements.

RÉSUMÉ

Un banc d'essai à multi-capteurs pour la détermination du débit d'absorption spécifique (DAS) dans le cas d'équipements sans fil émettant dans des tissus analogues à ceux du corps humain est présenté. Une estimation en temps réel des taux d'absorption spécifique est proposé, considerant un banc d'essai à multi-capteurs distribués spatialement. En comparaison d'un système comportant un robot multi-axial pour la mesure des DAS, celui qui est proposée ici ne requiert aucun déplacement, reduisant ainsi de manière drastique le temps d'acquisition, dès lors que des techniques parallèles d'acquisition de données et d'interpolation sont employées afin d'accélérer les mesures.

1. Introduction

The SAR (specific absorption rate), expressed in W/kg, describes the radio-frequency (RF) power absorbed per mass unit in a dielectric medium exposed to a given electric field $|E|$ (expressed in V/m), characterized by its electric conductivity σ (in S/m) and its mass density ρ (in kg/m^3).

$$SAR = \frac{\sigma \cdot |E|^2}{\rho} \text{ (W/kg)} \tag{1}$$

Any SAR value can consequently be deduced from electric fields measurement within a given dielectric medium, usually assumed as homogeneous for practical convenience. It is therefore necessary to reconstruct this incident *E*-field vector supported by three orthogonal electrical quantities, which have to be separately measured. Three co-localized orthogonal dipoles loaded by detection Schottky diodes are usually used for measuring the corresponding DC-voltage amplitudes, then

* Corresponding author.
E-mail address: christian.person@telecom-bretagne.eu (C. Person).

1631-0705/$ – see front matter
http://dx.doi.org/10.1016/j.crhy.2013.02.009

Fig. 1. Conventional SAR test bench with multi-axial robot and a 3D E-fields' detection probe [3].

allowing the reconstruction of the effective E-field value by summation, assuming the RF power amplitude being proportional to the square of the E-field (far-field conditions).

Different measurement and detection techniques have been investigated for recovering such electrical E-field (electro-optical conversion, quadratic detection, piezo, ...) with particular attention devoted to linearity, sensitivity, dynamic range, bandwidth capabilities, dimensions and distortion. EN 620209-1 and 620209-2, IEEE 1528, FCC standards [1,2] are based upon such E-field detection, requiring the use of 3D E-field scanners for reconstructing spatial E-field distribution with liquids reproducing human-tissue-equivalent electrical properties. One can imagine the boring operation, which has to be performed at each central operating frequency band of an emitting equipment (for normative RF output, powers greater than 20 dB m), along different use cases (cheek, tilted, body positions). Today, fast SAR calculation is discussed for accelerating the SAR acquisition process, through extrapolation techniques or using pre-identified critical E-field distributions. Unfortunately, if such techniques lead to SAR acquisition time reduction, they are also in contradiction with sensitivity and accuracy constraints, and cannot be fully compatible with standard requirements. Nevertheless, normalization committees examine intensively complementary techniques for overcoming such restrictions, with the expectation in a near future to offer a systematic SAR determination for any RF wireless equipment, then reinforcing security and health protection for customers.

2. A no-robot SAR test bench as an alternative issue

Fig. 1 describes a conventional SAR test bench based upon a conventional E-field probe, comprised of three orthogonal quadratic detectors for recovering x–y–z E-field components, immerged in a phantom filled with liquids reproducing human tissues' electrical properties.

A complete SAR characterization operation for a given multi-band mobile phone, for instance, corresponds to a full-day measurement tedious task, bringing non-negligible cost not compatible with mass-production constraints.

Therefore, we propose to combine E-field reconstruction techniques (interpolation extrapolation, prediction) with a spatial SAR simultaneous field acquisition. Namely, a multiprobe SAR test bench is developed and discussed in order to accelerate the electromagnetic fields measurement, without any mechanical operation (displacement, mobile positioning).

3. Planar x–y multiprobe SAR sensor for fast SAR assessment

A first approach has been proposed in [4], then [5] and [6], where five crossed probes (for x–y field-component measurements) were used, in combination with local E-field reconstruction using interpolating/extrapolating techniques. It was a preliminary fast SAR technique, based on a fixed scanned region in order to cover a representative exposed section of the phantom.

The basic idea was to proceed with a reduced number of appropriate and fixed position measurement points for a comparative SAR assessment, dedicated to post-production SAR verification. The effective SAR value is determined through a comparative analysis provided by a reference certified SAR measurement. A post processing is employed for accessing to the estimated SAR values.

The structure is based upon two crossed probes arrays (see Fig. 2), processed on an epoxy substrate ($\varepsilon_r = 4.3$) for minimizing cost production, interdigitated and assembled on a double-face printed circuit board (PCB) supporting interconnections towards connectors for digitalization and signal processing. Each crossed probes are composed of orthogonal

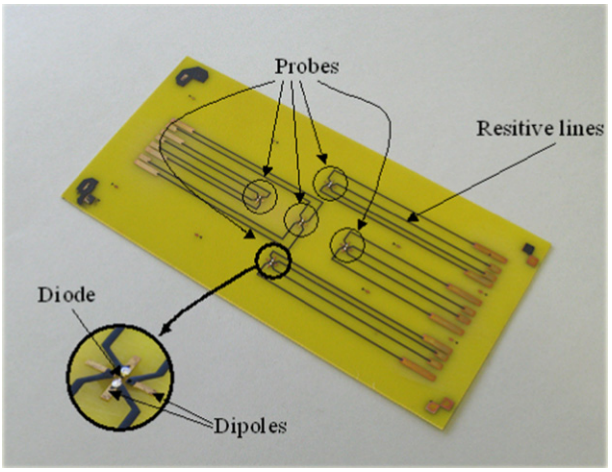

Fig. 2. Planar x–y multiprobe sensor.

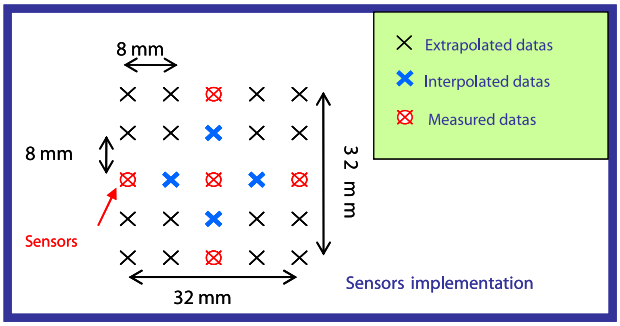

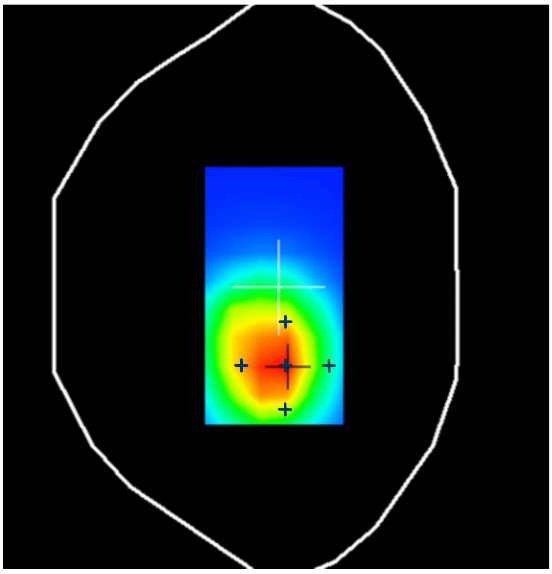

Fig. 3. Sensors implementation and surface field extraction illustration for a commercial mobile phone (measurement + extrapolation + reconstruction).

dipoles (for x–y planar detection) loaded by two SMD (surface mounted devices) miniaturized Schottky diodes (top–bottom PCB mounted).

The relative positioning, coupling and dimensions of such crossed-probes array have been optimized so as to ensure a perfectly controlled detection area, without modifying the SAR distribution due to the presence of the PCB. The periodicity of the sensors is described in Fig. 3, as well as the interpolated and extrapolated positions deduced by calculation after

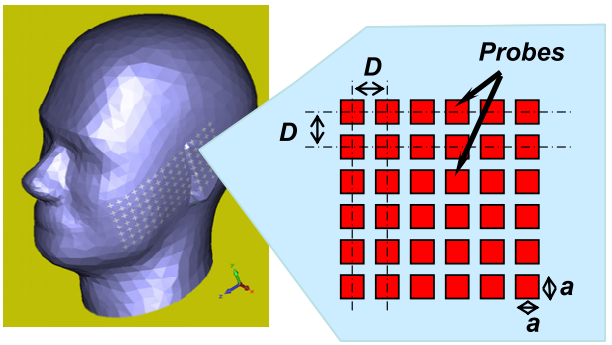

(a)

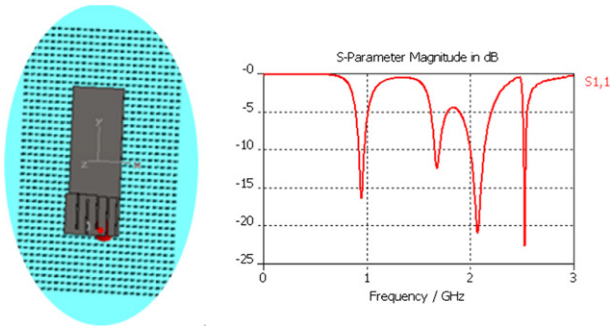

(b)

Fig. 4. (a) Multiprobe SAR test bench (only surface sensors reported here). (b) Description of the structure modelled on CST-MS™.

measurements. A 32×32 mm^2 surface can be analyzed, and the maximum SAR value can therefore be extracted after computation for any mobile equipment centered on this scanned area.

Note that this planar sensor can only measure spatial E-field distributions, assuming the E-field z-component can be deduced from theoretical liquid absorption and corresponding penetration depth. Consequently, the local maximum SAR value in a 10 g cube (typically $21 \times 21 \times 21$ mm^3) is determined from both theoretical and measured E-field parameters.

One has to note that the position of the mobile phone is deduced from the reference measure of the SAR distribution. That means that this position is predefined for each type of equipment, thus leading to a pre-estimated SAR uncertainty value. This procedure is completely appropriate on a production line for systematic SAR estimation of similar product series.

4. 3D multiprobe SAR test bench without robot

We investigated on a 3D multiprobe SAR test bench without robot, as illustrated in Fig. 4. The concept lies on the implementation of a planar or conformed E-field sensor network for accessing the 2D measured E-field distribution, completed by additional detection probes positioned along the z-penetration direction within tissues.

4.1. Parametric analysis

Note that the sensors positioning, their spatial mesh density and the probe dimensions have been studied in order to minimize the distortion of the local E-field distribution in the scanned reference place, and to prevent any parasitic coupling or interferences.

Fig. 5 shows the spatial E-field distribution when considering an illumination of a parallelepiped phantom with a reference PIFA antenna @ 900 MHz mounted on a PCB substrate. The elementary probes are modelled as miniaturized metallic pads (which support Schottky diodes – not considered here – for quadratic detection), with a periodicity D and square dimensions $a \times a$ (see Fig. 4).

We can observe that this worst case analysis (sensors assumed to be perfect metallic pads) do not distort significantly the SAR distribution. Of course, this phenomenon is intrinsically related to the sensors mesh density and dimensions and has to be accurately considered.

4.1.1. Incidence of the sensor dimensions $a \times a$ on the SAR

The position of the first layer of the 3D sensor array (outer surface) is critical as it is located close to the inner surface of the phantom for enhancing the sensitivity. It may consequently interfere with the RF emitting source (near-field coupling phenomena), but also modify the local E-field distribution.

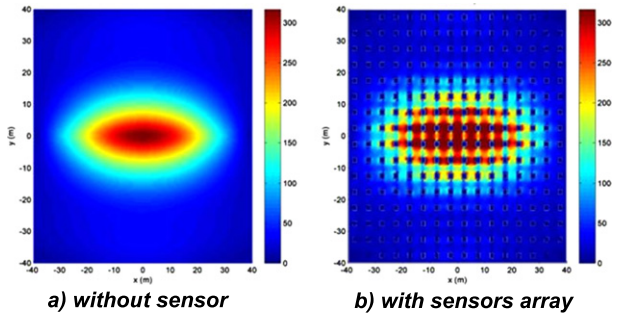

Fig. 5. 2D scanned area with/without miniaturized spatially distributed sensors – illumination with a PIFA antenna @ 900 MHz.

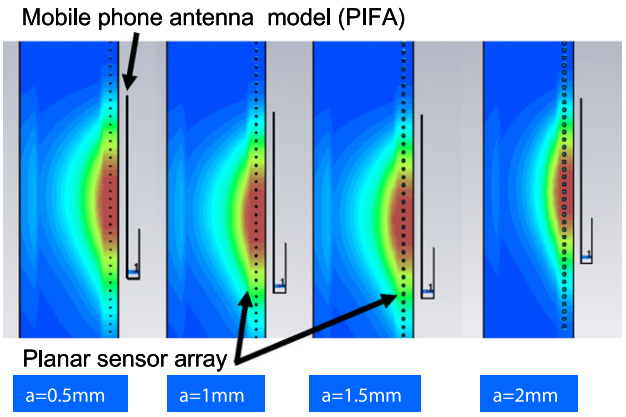

Fig. 6. Incidence of the sensors dimensions ($a \times a$) on the SAR distribution.

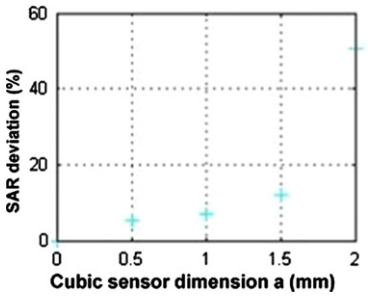

Fig. 7. Relative SAR deviation versus the $a \times a$ dimension of each sensor.

We have first carefully analyzed this incidence, through the 3D EM modelling procedure performed on CST – Microwave Studio™. A PIFA (printed inverted F shape antenna) is considered, positioned on a conventional PCB substrate (FR4 epoxy™), and placed 2 mm parallel to a rectangular phantom filled with equivalent normative head-liquid (standard EN 62209-1[1]). Fig. 6 exhibits the SAR distribution in the phantom (cross section) when varying the dimensions $a \times a$ of each square metallic sensor (perfect conductivity) of the planar x–y multi-sensor array.

We can observe that dimensions $a \times a$ less than 1×1 mm^2 induce a SAR deviation less than 10% @ 900 MHz. For increased frequency values, the dimension a should be kept lower than 1.5 mm for preventing SAR deviation, but the distance between the probe array location and the RF source is also critical and may be exploited to optimize the sensor array spatial resolution as a function of the frequency range to cover.

4.1.2. Incidence of a 2D sensor array position on the SAR

We consider a fixed probe array ($a = 2$ mm, $D = 5$ mm – see Fig. 4) and we analyze the effect of the distance between the source (placed against the outer part of the 2 mm-thick phantom shell) and the first planar sensor layer of the future 3D SAR test bench. Note that the worst case has been selected here ($a = 2$ mm), so as to consider the most significant effect of the sensors array in terms of waves reflection.

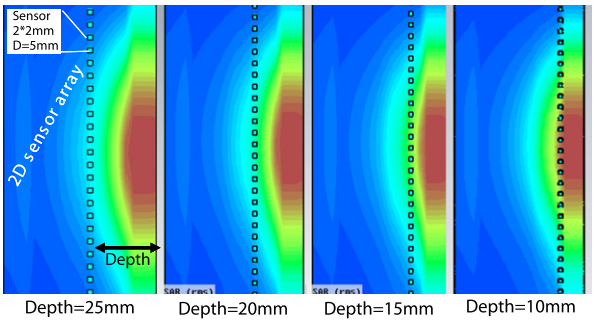

Fig. 8. Incidence of the 2D sensor array location (Depth) in the phantom on the SAR distribution.

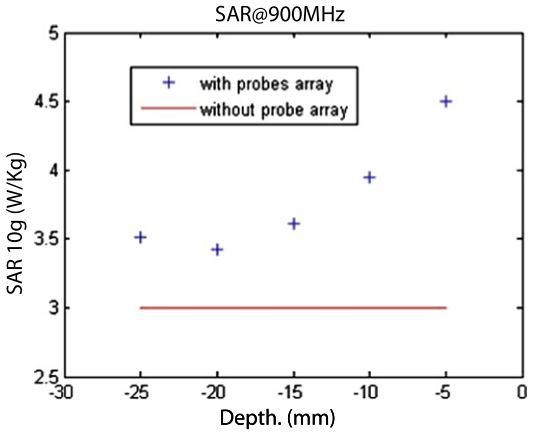

Fig. 9. Relative SAR deviation versus the position depth of a planar array versus the RF source.

The SAR deviates from the reference SAR value (obtained without the probe array), indicating the minimum distance to be maintained for preventing any distortion. The worst critical case is presented below (@ 900 MHz), exhibiting an achievable 10% deviation for a depth positioning between 10 to 20 mm from the outer phantom surface.

4.1.3. Spectral reconstruction with plane wave superposition

Knowing the distribution of the tangential x–y components of a reference plane (the one containing the probe array), the spectral reconstruction is used to calculate the distribution of the orthogonal z-component to this plane. Moreover, when the electrical properties of the medium are known, this method can reconstruct the field throughout the volume. The spectral reconstruction is an appropriate technique for the reconstruction of the near field in a homogeneous and isotropic medium.

The electric field can be decomposed by superimposing an infinite number of plane waves propagating in all directions of the half-space. For each direction, two plane waves, one polarized so that its electric field vector is contained in the plane orthogonal to the measurement plane, the other polarized so that its electric field vector is orthogonal to the vector wave and to the plane orthogonal to the measurement plane. The relative amplitudes to this pair of plane waves $P_{x,y}$ are given below:

$$\begin{Bmatrix} P_x(k_x,k_y) \\ P_y(k_x,k_y) \end{Bmatrix} = \iint_{\Re^2} \begin{Bmatrix} E_x(x,y,0) \\ E_y(x,y,0) \end{Bmatrix} \cdot e^{\mathrm{j}(k_x\cdot x + k_y\cdot y)}\,\mathrm{d}x\,\mathrm{d}y \tag{2}$$

with k_x, k_y propagation constants along x and y axes, respectively.

Once plane wave amplitudes are calculated, the three components of the electric field can be calculated for any point in the considered volume by propagation or back-propagation of these waves (Eq. (3)).

$$\begin{Bmatrix} E_x(x,y,z) \\ E_y(x,y,z) \\ E_z(x,y,z) \end{Bmatrix} = \frac{1}{(2\pi)^2} \iint_{\Re^2} \begin{Bmatrix} P_x(k_x,k_y) \\ P_y(k_x,k_y) \\ [-\frac{k_x}{k_z}\cdot P_x(k_x,k_y) - \frac{k_y}{k_z}\cdot P_y(k_x,k_y)] \end{Bmatrix} \cdot e^{-\mathrm{j}(k_x\cdot x + k_y\cdot y + k_z\cdot z)}\,\mathrm{d}k_x\,\mathrm{d}k_y \tag{3}$$

In the case of a dielectric medium with losses, waves are attenuated during their propagation. This attenuation is expressed mathematically by a complex wave vector, but perfectly controlled thanks to the perfect control of the equivalent liquid electrical properties.

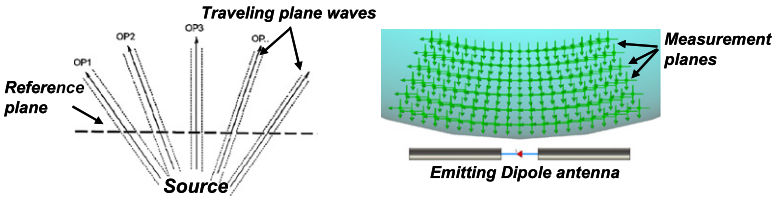

Fig. 10. Superposition of plane waves: Principle and application.

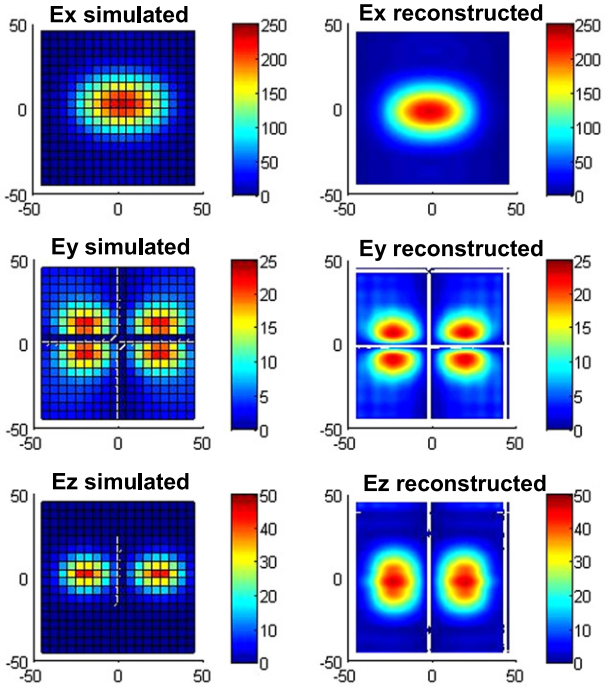

Fig. 11. Phantom illuminated with a dipole source antenna – comparisons between ideal simulated and reconstructed fields components.

The reconstruction by Fourier transform has been given above in its integral form, that is to say, in the case of a distribution that can be expressed by mathematical functions and provided the integral can be performed. In reality, the field components tangential to the measurement plane will be measured at discrete points. In addition, there will be a truncation of the measurement surface itself caused by the truncation of the measurement volume. Reconstruction must be made through a discrete Fourier transform or even using the algorithm of fast Fourier transform (FFT).

A simple dipole antenna was simulated to validate the algorithm. The antenna is placed at a distance of 5 mm from a parallelepiped phantom filled with liquid. “Virtual sensors” are then introduced into an intermediate plane of the phantom. The 3D electromagnetic simulator CST Microwave Studio™ allows us to place “probes” to recover the vector quantity associated with the electric field components at a given point. The values of each component for each point are then exported as ASCII files using a Visual Basic macro. These files are then processed with Matlab™ to perform the field reconstruction.

These reconstruction procedure exhibits quite good results in accordance with the reference simulated fields, as described in Figs. 10 and 11, which correspond to a dipole and a PIFA antenna, respectively. Remind that the z component (normal to the measurement plane) is reconstructed from the two other x–y components.

The reconstructed field components are completely similar to the ideal expected ones, underlying the robustness of the reconstruction technique, and validating the fact that the SAR calculation can be based upon hybrid field components deduced from both simulations and measures.

Spatial E-field distributions can be real-time reconstructed, and SAR computation can be performed, considering the predicted and well-controlled liquid absorption (the liquid in which probes are inserted to reproduced human tissues' properties).

4.2. Prototype and implementation

The previous planar array brings some difficulties in terms of miniaturization capabilities as well as interferences and parasitic coupling between sensors and resistive feeding lines as they are both located on the same level.

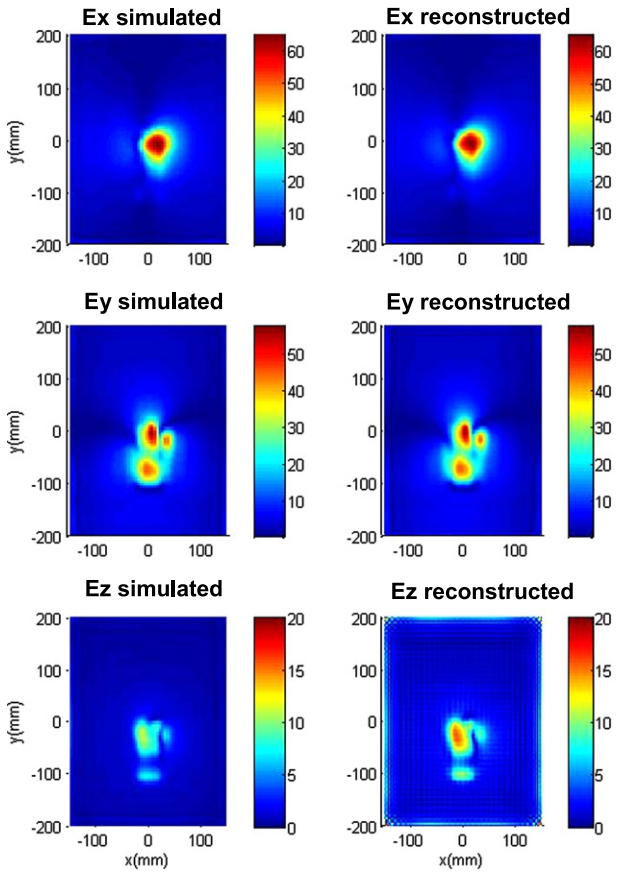

Fig. 12. Phantom illuminated with a PIFA source antenna – comparisons between ideal simulated and reconstructed fields components.

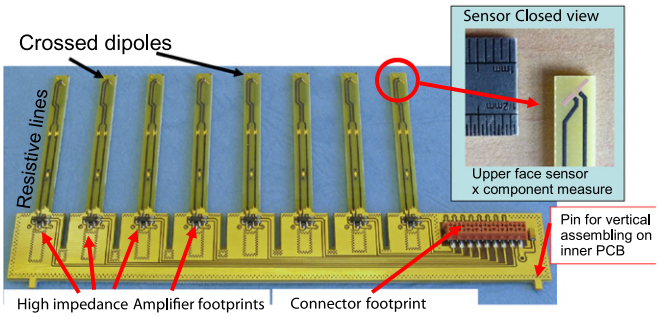

Fig. 13. Details of a linear probe array with amplifier interfaces.

Consequently, we investigated on a 3D multiprobe prototype with vertically positioned sensors, assembled and interconnected to signal processing and digitalization interfaces by means of a PCB. The 3D probes positioning can be easily achieved by considering different heights for sensors through different access lines and supporting substrate lengths.

A 3D scanned area, with measured x–y–z E-field components, is ensured through vertically positioned crossed probes arrays (for orthogonal x–y components detection) and height position variability for z-component determination.

Low-cost material PCB substrates are employed for cost production reduction. A bottom PCB is used for interconnections towards numerical interface (digitalization and signal processing such us interpolation techniques and data analysis optimization procedures).

Sixty-seven probes (in the example given in Fig. 15) recover x–y electric field components in a given reference plane, converting them into analogue DC voltage for digitalization.

A 64×112 mm^2 scanned area is achieved, corresponding to typical dimensions to be covered for generic smart phones. The sensors array is connected with a multiple inputs digitizer (from National Instruments™ NI6255 [6]), thus enabling direct detection of 60 voltages on each interface.

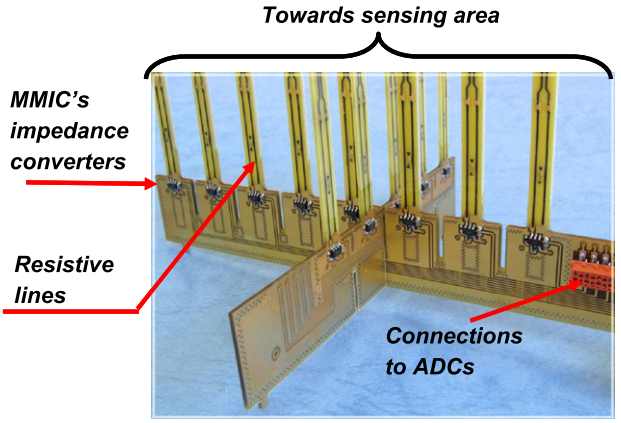

Fig. 14. Basic linear probes array with amplifiers and connectors footprints for interconnections.

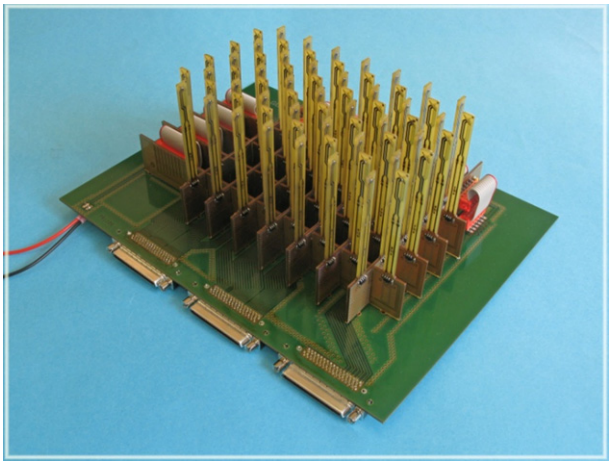

Fig. 15. Assembled multiprobe SAR test bench (without packaging and phantom).

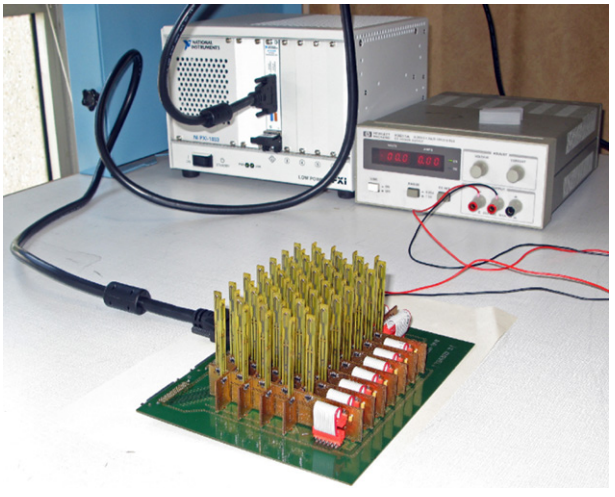

Fig. 16. Test bench with parallel signal digitalization.

One hundred and thirty-four analogue voltage levels have to be recovered with the test-set depicted in Fig. 16, while the commercial version developed by Satimo [3] will support more than 600 sensors for a 230×230 mm^2 scanned area. A specific multiplexing interface, monitored by a micro-controller, is required for addressing such number of analogue inputs.

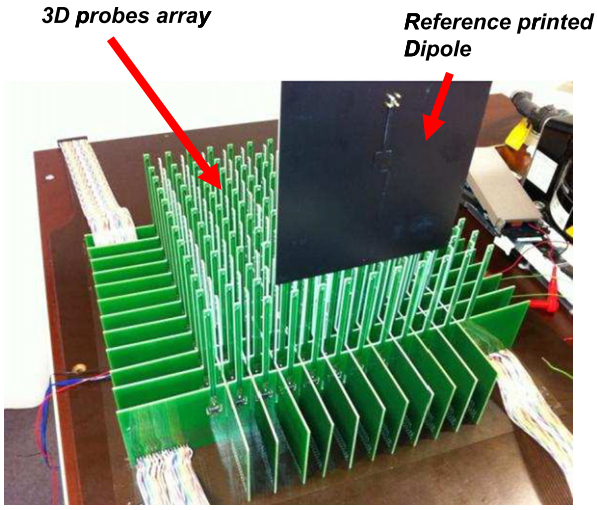

Fig. 17. 3D probes array calibration with a reference printed dipole.

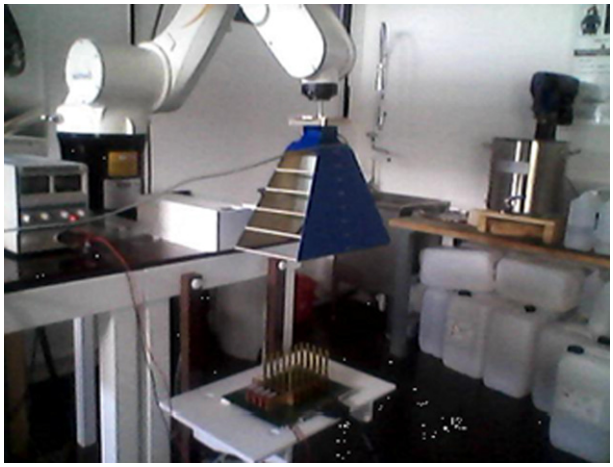

Fig. 18. Calibration test bench with a waveguide horn.

4.3. Calibration procedure

One critical point for developing such multi-sensors system concerns the calibration. Conventional E-field probes are characterized using normalized techniques. For each elementary quadratic sensor, the coefficient calibration $K_{\text{sensor}\,i}$ – see Eq. (4) – has to be computed, by comparing an incident perfectly controlled E-field ant the corresponding output DC voltage measured. Namely,

$$K_{\text{sensor}\,1} = \frac{V_{\text{measured}}}{E^2_{\text{theoretical}}} \tag{4}$$

The incident E-field illuminating each sensor must be properly controlled, both in terms of magnitude, polarization, and angular orientation. We investigate two methods that were previously discussed in [7].

A calibration method with a reference dipole can be considered. This technique appears as quite sensitive and induces complex operations considering the huge number of positions to consider for identifying all polarization and x–y–z probe positions.

We select a more general method, using a reference wideband horn antenna [3], which appears more appropriate to accelerate calibration procedure. The E-field of the horn antenna has been measured in a reference near-field surface plane using a pre-calibrated probe.

Once incident E-field components are completely defined in a pre-defined reference plane, two measurements steps are required for measuring the detected voltages for both polarization through a 90° rotation of the probes array.

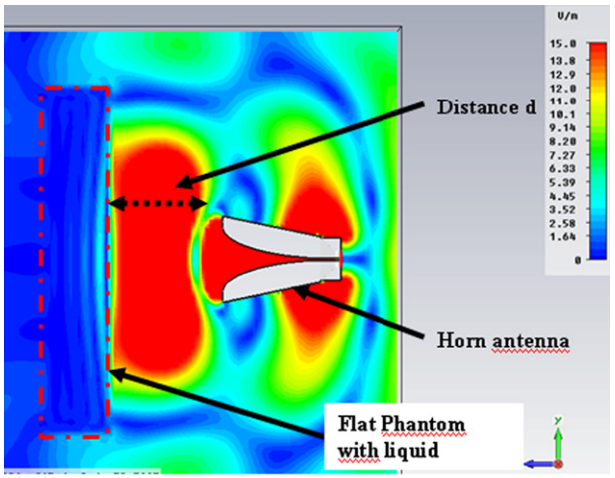

Fig. 19. *E*-field distribution within a flat phantom illuminated by the SH 800 horn at 900 MHz (distance horn aperture–simulated planar area: *d*).

One important issue is the relative homogeneity of the *E*-fields' distribution in the sensors calibration plane. Simulations on HFSS™ have been performed to verify the *E*-fields' distribution at different distances from the radiating horn aperture. A homogeneous plane wave distribution is observed at a distance of about 20 cm for mobile phone frequencies.

The presence of the phantom in front of the horn aperture (flat phantom filled with an equivalent liquid) do not degrade the spatial *E*-field distribution, which can be considered as a planar plane wave with corresponding transversal field components.

The voltage responses can therefore be determined for each sensor independently of their positions versus the incident E-field illumination strength (V/m) at one selected frequency (900 MHz here), and for one polarization. An instantaneous measurement is made using multi-access ports digitalization interfaces and direct computation for extraction of the equivalent coefficients K_i.

5. Assembled multi-sensors SAR system

Finally, we proceeded with the integration of such 3D multi-sensors SAR system, assembled with a phantom head (child head) by exploiting stereo-lithography techniques with low permittivity low loss resins. Fig. 20 describes the different part of the finalized prototype with the phantom.

The probes array is inserted in the phantom so as to ensure close vicinity between the inner shell of the phantom and the sensors detecting area. This is easily achieved with the proposed system by modifying the length of each sensor individually, depending on its position in the array, and with respect to the phantom inner surface.

This corresponds to the first version of a completely integrated SAR system for real-time SAR assessment.

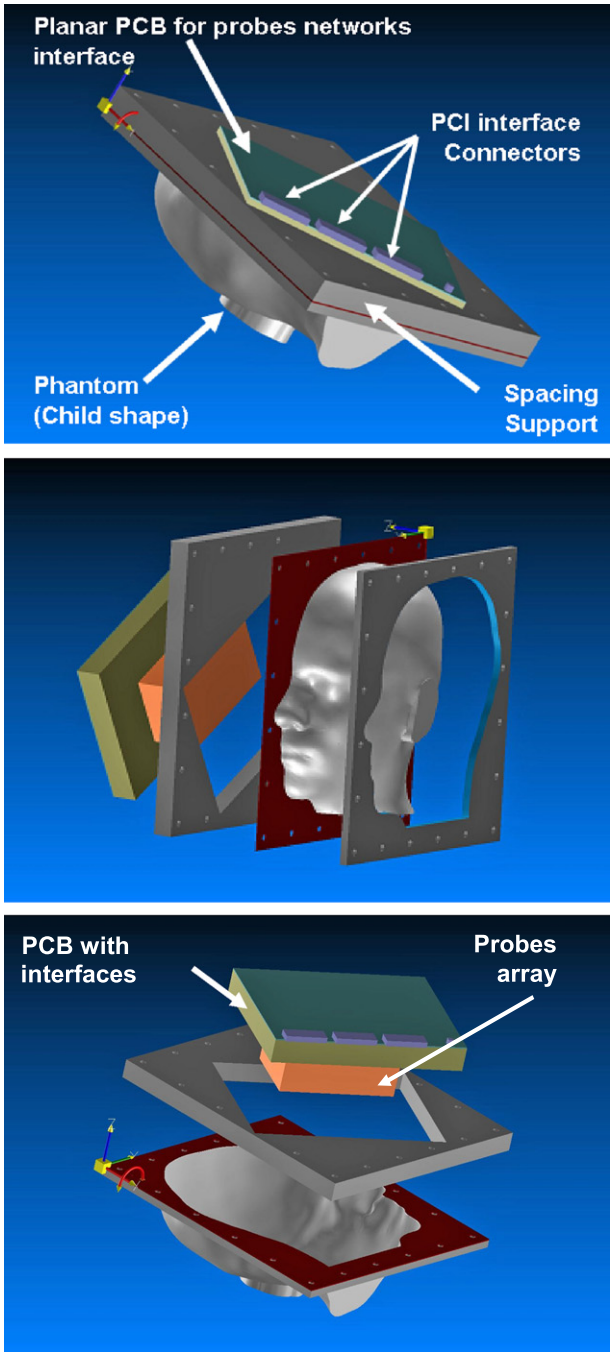

Fig. 20. Description of the 3D no-robot SAR system with human head phantom.

6. Conclusion

In this paper, we present a 3D multi-sensor system for real-time SAR assessment. The prototype has been optimized by carefully analyzing the incidence of the probes array on the SAR distribution, so as to produce a relative error less than 10% with respect to normative SAR measurement approaches.

One original aspect of this work concerns the design and realization of the probe arrays, with low-cost assembling techniques and innovation on the spatial distribution of the sensors. Another innovation concerns the introduction of this array with a human head phantom so as to be as representative as possible to compliance tests.

Such system should be attractive for both mobile phone manufacturers and distributors for real-time SAR assessment.

Acknowledgements

This work has been supported by the National Research Agency ANR in France, through the project "Merodas" [8]. The authors thank Ismaël Pelé from Satimo for the EM simulations and results.

References

[1] ICNIRP Guidelines, Guidelines for limiting exposure to time-varying electric, magnetic, and electromagnetic fields (up to 300 GHz), Health Phys. (April 1998).
[2] IEC Standard, Human exposure to radio frequency fields from hand-held and body-mounted wireless communication devices – Human models, instrumentation, and procedures. Part 2: Procedure to determine the specific absorption rate (SAR) in the head and body for 30 MHz to 6 GHz handheld and body-mounted devices used in close proximity to the body, IEC 62209-2, 2008.
[3] www.satimo.fr.
[4] S. Boucher, C. Person, F. Le Pennec, R. Butet, G. Toutain, Y. Toutain, V. Vigneras, E. Hamon, Specific apparatus for post-production SAR evaluation through differential measurements, in: Bioelectromagnetics Symposium 2008 – BEMs2008, San Diego, California, USA, 7–12 June 2008.
[5] S. Boucher, et al., Fast post-production SAR evaluation system through a comparative *E*-fields extraction procedure, in: European Microwave Conference EuMC2008, Amsterdam, October 2008.
[6] http://sine.ni.com/nips/cds/view/p/lang/en/nid/201605.
[7] Gaetan Guevel, Romain Butet, Sylvie Le Dall, Yann Toutain, Joe Wiart, Christian Person, in: Calibration Techniques for Multi-Sensor SAR Systems, 6th European Conference on Antennas and Propagation EuCAP 2012, Prague, 26–30 March 2012.
[8] http://whist.institut-telecom.fr/meroda.